
Article:
Wigley, B.R., Stillman, E.C. and Craig-Atkins, E. (2024) Taking shape: A new geometric morphometric approach to quantifying dental fluctuating asymmetry and its application to the evaluation of developmental stress. Archaeometry, 66 (6). pp. 1399-1423. ISSN: 0003-813X

https://doi.org/10.1111/arcm.12973

Received: 23 August 2023 | Accepted: 21 March 2024

DOI: 10.1111/arcm.12973

ORIGINAL ARTICLE

Taking shape: A new geometric morphometric approach to quantifying dental fluctuating asymmetry and its application to the evaluation of developmental stress

Ben Wigley [1,2] | **Eleanor Stillman** [2] | **Elizabeth Craig-Atkins** [1]

[1]Department of Archaeology, University of Sheffield, Sheffield, UK

[2]School of Mathematics and Statistics, University of Sheffield, Sheffield, UK

Correspondence
Ben Wigley, Department of Archaeology, University of Sheffield, Sheffield, UK.
Email: b.r.wigley@sheffield.ac.uk

Funding information
This work was supported by the Arts & Humanities Research Council (179466810 AH/R012733/1) through the White Rose College of the Arts & Humanities.

Abstract
Although evaluating developmental stress is challenging, it is critical to understanding phenotypic adaptation and differentials in morbidity and mortality related to spatiotemporal variation in environmental and cultural factors. This paper presents a new, reproducible, and reliable geometric morphometric (GM) protocol through which stress-induced deviations to symmetry, known as fluctuating asymmetry (FA), can be robustly quantified. A case study, in which maternally mediated early-life stress in human skeletal remains is explored through first permanent molar (M1) FA, illustrates the method's effectiveness and wide-ranging potential to revolutionise the investigation of themes such as stress intensity, developmental processes, and buffering mechanisms in past populations.

KEYWORDS
developmental stress, first permanent molar, fluctuating asymmetry, geometric morphometrics, mother–child nexus

INTRODUCTION

A stressor creates "an increased demand upon the body to readjust itself" and "requires adaptation to a problem" (Selye, 1973: 693). In other words, stress disrupts the efficient deployment of resources and forces physiological modifications in order to return to homeostasis. Because physiological responses to stressors are nonspecific with the nature of the stimulus itself being largely immaterial, it is the intensity of the stress experience that is important in defining how

much disruption is caused (Escós et al., 2000; Selye, 1973). Stress experience also reflects how well adapted an individual or group is to its environment as well as the ability to mitigate deleterious influences and is therefore a measure of fitness and resilience (or frailty) (Graham & Ozener, 2016; Graham et al., 2010; Klingenberg, 2015; Orr, 2009; Vaupel, 1988). Quantifications of stress intensity are consequently fundamental to many investigations in the life sciences, including those conducted by biological anthropologists and bioarchaeologists (e.g., Armelagos et al., 2009; DeWitte & Wood, 2008; Temple, 2014).

Developmental stress, which can be defined as nonspecific physiological disruptions to growth trajectories experienced before the attainment of somatic maturity, is of particular interest due to the impact it has on phenotypic outcomes. For example, stressors experienced during fetal and early-postnatal development have been implicated in substantial differentials in growth, morbidity, and mortality in both clinical studies (Lopuhaa et al., 2000; Ravelli et al., 1998; Roseboom et al., 2000, 2001) and bioarchaeological research (Armelagos et al., 2009; DeWitte & Wood, 2008; Temple, 2014). Reconstructing developmental experiences and quantifying stress intensity can be challenging, however, especially in archaeological samples. For instance, although it may be plausible to assess the activation of the hypothalamic–pituitary–adrenal axis and changes in cortisol levels—that is, the "stress hormone"—in living samples in response to developmental adversity (Betts et al., 2017; Edwards & Boonstra, 2018), retrospectively gauging hormonal fluctuations in archaeologically recovered skeletal materials has met with mixed results. Although cortisol has been detected in archaeological remains, including dental enamel (which is laid down during development and does not remodel in later life), survival is variable and assessment is dependent upon destructive analyses (Quade et al., 2020; Webb et al., 2010). Similarly, although stress-induced and durable changes to genome expression (e.g., DNA methylation) are thought to be responsible for variation in later-life outcomes (Cao-Lei et al., 2014; Vaiserman, 2015), the analysis of genetic materials is still limited by taphonomic factors such as contamination and degradation, and, due to the requirement for specialist equipment, is often not a practical option (Briggs et al., 2010; Green et al., 2009; Höss et al., 1996; Klaus, 2014; Pruvost et al., 2005).

In summary, although of great importance, the in vivo redeployment of physiological resources during development in response to stress can be incredibly hard to measure effectively, particularly in past populations. One potential way of overcoming this obstacle is by driving forward methodological improvements in how stress-induced deviations from perfect symmetry, known as fluctuating asymmetry (FA), are captured and evaluated (Graham et al., 2010; Klingenberg, 2015; Van Valen, 1962). This paper will describe a reproducible and adaptable method through which FA can be quantified through geometric morphometric (GM) methods.

BACKGROUND

Fluctuating asymmetry

Symmetry is the result of repetition via a reversible transformation (e.g., reflection) that maps every point of an object onto another point in the same plane or space. As repetition of features in the ontogenetic process is energetically efficient and therefore adaptively advantageous, symmetric development is a trait common to many organisms (Graham et al., 2010; Klingenberg, 2015). Reflection of an object about a median plane creates bilaterally symmetric traits (i.e., a mirror image). In the case of object symmetry, the structure itself is symmetric and the plane of reflection passes through it (e.g., the face). Whereas, for matching bilateral symmetry, two copies of a structure are present, one each side of the median plane (e.g., left and right teeth) (Graham et al., 2010; Klingenberg, 2015). Symmetry is, however, dependent upon developmental homeostasis (i.e., the precise allocation of somatic resources needed to

maintain developmental trajectories) and is thus vulnerable to stressors, which can create asymmetries due to the disruption they cause to normal physiological processes (Graham et al., 2010; Klingenberg, 2015; Schmalhausen, 1949; Waddington, 1957).

In bilateral traits there are three commonly referenced types of asymmetry that were formally defined by Van Valen (1962). These are directional asymmetry, antisymmetry, and fluctuating asymmetry (the latter two referred to collectively as nondirectional asymmetry). If a trait is directionally asymmetric, there is a consistent bias toward one side. The normal location of the human heart on the left side of the body is an example of directional asymmetry. When asymmetry is evaluated on a continuous scale with a signed measure, directional asymmetry produces a skewed distribution (Graham et al., 2010; Klingenberg, 2015; Van Valen, 1962) (Figure 1). Antisymmetry, by contrast, is a pattern of asymmetry in which sinistral and dextral forms are equally common. Though not readily evident in humans, antisymmetry can be seen in a variety of plants and animals (e.g., differences in claw size in male fiddler crabs) and in a signed continuous measure is associated with bimodal or, in more subtle cases, platykurtic distribution (Graham et al., 2010; Klingenberg, 2015; Van Valen, 1962). Fluctuating asymmetry, meanwhile, is the result of random deviations in the developmental process from a "target phenotype" with perfect symmetry. Deviations, which can be viewed as developmental errors, are typically stress induced and without functional consequence, and, in a signed measure, produce symmetric distributions with a mean of 0 (i.e., errors are equally likely to occur on either the left or right side) (Klingenberg, 2015; Graham et al., 2010; Van Valen, 1962). Due to this association with developmental stress, FA has often been employed as a stress marker (e.g., Barrett et al., 2012; Guatelli-Steinberg et al., 2006; O'Donnell & Moes, 2020). However, the relationship between FA and stress can be complicated by buffering mechanisms that mitigate stressors, and FA is more correctly considered a measure of developmental instability and a proxy for developmental stress (Graham et al., 2010; Klingenberg, 2015).

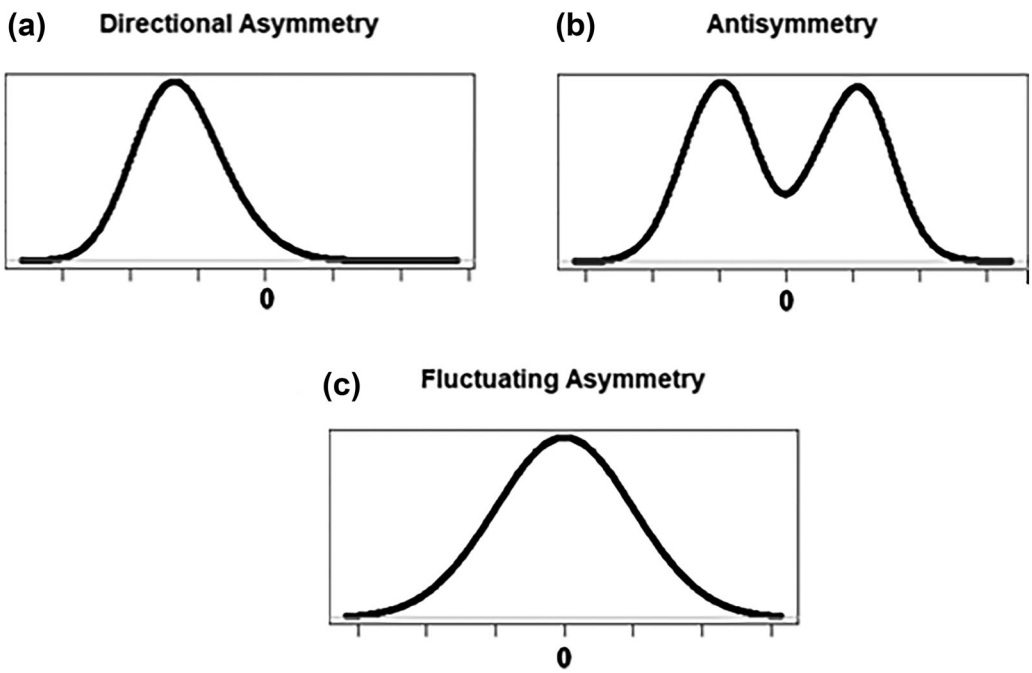

FIGURE 1 The distributions associated with directional asymmetry (a), antisymmetry (b), and fluctuating asymmetry (c) in a signed univariate measure.

FA has been employed diversely in many life sciences. Dental FA, for example, has been utilised to investigate themes such as environmental stress, physiological frailty, and resilience in both living and archaeologically recovered human samples (Barrett et al., 2012; Guatelli-Steinberg et al., 2006; O'Donnell & Moes, 2020). Although this work has generally validated the hypothesis that groups exposed to adverse and physiologically stressful environments during development exhibit higher FA (Barrett et al., 2012; Guatelli-Steinberg et al., 2006; Perzigian, 1977), in other respects it has met with mixed results and failed to fulfil calls for FA to be robustly linked to conventional measures of fitness (Bailit et al., 1970: 635–636). To illustrate, in an early study Townsend and Brown (1980) found significant differences in dental FA between Indigenous Australian females and males participating in a longitudinal growth study and hypothesised this was associated with well-established sex differentials in frailty (DeWitte, 2010; Stinson, 1985). However, in later work, O'Donnell and Moes (2020) failed to detect any disparity between sexes in the remains of ancestral Puebloans, whereas Guatelli-Steinberg et al. (2006) reported significant differences in FA between females and males in certain teeth in a mixed sample containing prehistoric Indigenous American hunter-gathers and agriculturalists as well as members of a politically marginalised 20th century community. Although the variability in results must to a certain extent reflect the diversity of samples analysed and the impact of contextually specific factors, limitations, and differences in methodologies that developed over time likely also play a part. Even though all these projects used simple linear measures of buccolingual and mesiodistal diameter, Townsend and Brown (1980) utilised correlation coefficients to quantify asymmetry and aggregated sex cohort scores for comparison, whereas O'Donnell and Moes (2020) compared individual composite z-scores. In contrast, Guatelli-Steinberg et al. (2006) took a more statistically sophisticated approach and decomposed variation through a factorial ANOVA.

This variability in methods has been encountered through the full range of disciplines that study asymmetry. Reference, for example, can be made to the work of Palmer (1994) and Palmer and Strobeck (2003) to better appreciate the methodological diversity associated with past research. In the first of these primers, designed to facilitate the quantification and analysis of asymmetry, 13 separate methods of calculating FA are presented (Palmer, 1994). In the updated version, a further five have been added to what Palmer and Strobeck (2003) refer to as an "increasingly bewildering array" of metrics. Although both texts acknowledge that not all of these measures are of equal value (Palmer, 1994; Palmer & Strobeck, 2003), the plethora of options has limited comparability and fostered an atmosphere of uncertainty regarding the investigative utility of FA. In a meta-analysis by Leung and Forbes (1996), which collated data from both plant and animal studies, the authors concluded that although likely not spurious, the inconsistencies produced by past research meant that only weak relationships could be discerned among FA, stress, and fitness. Similarly, Møller's (1999) meta-analysis found that the statistical connections identified between FA (in plants, animals and humans) and outcomes in growth, fecundity, and mortality, although meaningful, were relatively weak. In sum, although theoretically FA should be an invaluable interrogative metric, the data collection and statistical protocols through which it is recorded and analysed need to be rigorously developed and tested before its full potential can be realised.

Geometric morphometrics methods

With advances in the field of morphometrics and the increasing accessibility of digitization/analytical software, it has become apparent that small variations, such as those associated with FA, are more readily detected in measures of shape than size (Adams et al., 2004; Bookstein, 1991; Klingenberg & McIntyre, 1998). Consequently, it has been proposed that greater standardisation and sophistication can be achieved by taking geometric morphometric

(GM) approaches (Graham et al., 2010; Klingenberg, 2015). Among the suite of GM methods available, coordinate-based methods have become popular among those wishing to explore anatomical variation (e.g., Klingenberg & McIntyre, 1998; Oxilia et al., 2021; Smith et al., 1997). These define shapes through configurations of Cartesian points placed at homologous landmarks and along outlines (Bookstein, 1997; Dryden & Mardia, 1998). After configurations are superimposed and semilandmarks handled to produce a point-to-point correspondence, Procrustean procedures relocate, rescale, and rotate configurations to minimise differences attributable to location, size and orientation (Dryden & Mardia, 1998; Gower, 1975). Through this process, shape variation is isolated and configurations registered in Kendall's shape space with the differences between them expressible as distances (Dryden & Mardia, 2016; Kendall, 1984; Klingenberg, 2020). Such procedures represent a practical, but in many fields, as of yet underexploited, method of investigating FA and therefore developmental stress.

An archaeological case study: maternally mediated, early-life stress

Arguably, the reconstruction of maternally mediated, early-life stress in past human populations, is one area to which a more sophisticated approach could make a significant contribution. Clinical research has shown that the first 1000 days postconception are critical in defining life-course trajectories (Barker, 2012; Gowland, 2015). Individuals who experienced severe nutritional deprivation during the Dutch Famine (AD 1944–1945) while maternally dependent illustrate this point. It has been found, for example, that those who endured the famine in mid-to-late gestation were significantly smaller at birth that those conceived post-famine and in later-life had a higher risk of cardiovascular, respiratory, and metabolic morbidity as well as higher mortality rates up to 50 years of age (Gowland, 2015; Lopuhaa et al., 2000; Ravelli et al., 1998; Roseboom et al., 2000; Roseboom et al., 2001). Despite the demonstrable importance of maternally mediated stress in affecting life-course trajectories in growth, morbidity, and mortality, investigating early-life perturbations in skeletal samples is difficult. As mentioned previously, in vivo epigenetic processes implicated in phenotypic programming survive poorly (Briggs et al., 2010; Cao-Lei et al., 2014; D'Urso & Brickner, 2014; Green et al., 2009; Höss et al., 1996; Klaus, 2014; Pruvost et al., 2005; Vaiserman, 2015), the remains of perinates represent a biased cohort of non-survivors (DeWitte & Stojanowski, 2015; Wood et al., 1992) and remodelling of bone can obscure the traces of early-life developmental stress in skeletally mature individuals (Hodson & Gowland, 2020; Lewis, 2017). Moreover, the nonspecific stress markers frequently employed by bioarchaeologists largely reflect childhood or later-life experience. Linear defects in the imbricational enamel of teeth and cranial porosity, for example, are associated with childhood stress (Brickley, 2018; Primeau et al., 2015). Meanwhile, as bone remodels throughout life, periosteal new bone formation often reflects physiological disruptions nearer to time of death (Weston, 2008). Therefore, for those investigating past populations the direct interrogation of early-life stress, transgenerational maternal influences and phenotypic plasticity are exceptionally challenging (Barker, 2012; Gowland, 2015; Klaus, 2014).

It may, however, be possible to explore early-life stress in past populations through FA in first permanent molars (M1s). M1s have matching bilateral symmetry (i.e., left and right antimeres are reflections of one another), and the development of occlusal features begins in utero (at approximately 16 weeks). Although wear can erode the occlusal surface, crowns do not remodel after mineralization, and therefore phenotypic variation in M1 occlusal morphology has the capacity to preserve maternally mediated, early-life stress in archaeological samples (Antoine & Hillson, 2016; Brickley et al., 2020; Harris, 2016; Hillson, 1996; Hillson, 2005; Lynnerup & Klaus, 2019). To the authors' knowledge, a GM analysis of M1 occlusal FA has not been attempted previously, and, likewise, FA has not been employed to interrogate directly

the impact of maternal influences on developmental stress in a bioarchaeological project. The aims of this paper are therefore first to demonstrate that M1 FA can be quantified through GM techniques. From there, FA differences in an archaeologically recovered human sample are explored to validate the assumption that M1 FA can advance the study of transgenerational expression of developmental stress. Finally, the capacity for GM evaluations of FA to shed light on developmental processes retrospectively is articulated.

MATERIALS

Archaeological human remains from 217 individuals dating from c. A.D. 750–1850 were analysed. They derived from four English sites: The Black Gate cemetery, Newcastle; St Hilda's Church, South Shields; St Lawrence's Church, Warwick; and York Barbican. These individuals provided 154 pairs of maxillary first permanent molars (M^1) and 148 mandibular (M_1) pairs; 85 skeletons had both. A total of 112 (51.9%) individuals had long bones with fully fused epiphyses and were therefore classified as skeletally mature, whereas 104 (48.1%) had long bone epiphyses that were not fully fused and were categorised as skeletally immature (Schaefer et al., 2009; Scheuer & Black, 2000). Eighty-five mature individuals were successfully assessed for skeletal sex using dimorphic traits in the pelvis and cranium (Buikstra & Ubelaker, 1994; Ferembach et al., 1980; White & Folkens, 2005); 36 (42.4%) were estimated to be female and 49 (57.6%) male.

METHODS

Digitisation

To produce images of M1 occlusal surfaces, a Canon EOS 250D DSLR camera with an AET-CS Auto Extension Tube was set to take JPEG images and affixed to a Kaiser Copy Stand. The imaging procedure developed (APPENDIX S1: DATA ACQUISITION AND ANALYSIS) ensured the consistent and stable alignment of both the photographic equipment and teeth (Cucchi et al., 2011: 15; Gómez-Robles et al., 2007; Gómez-Robles et al., 2008), accommodated the reflective qualities of enamel (Uzunov et al., 2015), and mitigated factors such as parallax error (Dukić, 2014; Mullins & Taylor, 2002). Replicate measures (which encompassed the photographic process from initial tooth placement onward) were taken to assess the impact of observer error and produce a mean shape to mitigate error when computing individual FA scores. So that images of left and right sides were directly comparable, the left was reflected.

Following imaging, homologous landmarks on the occlusal surface (Tables 1–2 and Figure 2) and an outline were digitised in the R environment (Wood et al., 1983; Wood & Engleman, 1988). Each outline was subsampled by $j = 1, \ldots, q < k$ equally spaced semilandmarks (discussed below) (Adams et al., 2021: 117–119; Olsen, 2015; Olsen & Westneat, 2015; R Core Team, 2023). At the end of the digitisation process, the occlusal surface of each tooth was represented by a k x m matrix (X) of Cartesian coordinates points, such as

$$X = \begin{pmatrix} x_1 & y_1 \\ x_2 & y_2 \\ \vdots & \vdots \\ x_k & y_k \end{pmatrix}$$

TABLE 1 Maxillary first permanent molar landmarks.

No.	Description
1	The center of the mesial fovea, at the most mesial extension of the sagittal fissure
2	The intersection of the sagittal fissure by the buccal fissure
3	The intersection of the sagittal fissure by the lingual fissure
4	The centre of the distal fovea located at the most distal extension of the sagittal fissure
5	Paracone apex
6	Metacone apex
7	Protocone apex
8	Hypocone apex

TABLE 2 Mandibular first permanent molar landmarks.

No.	Description
1	The centre of the mesial fovea, at the most mesial extension of the longitudinal fissure
2	The intersection of the longitudinal fissure by the mesiobuccal fissure
3	The intersection of the longitudinal fissure by the lingual fissure
4	The intersection of the longitudinal fissure by the distobuccal fissure
5	The distal fovea located at the most distal extension of the longitudinal fissure and, when present, its intersection with the buccal and lingual foveal fissures
6	Protoconid apex
7	Hypoconid apex
8	Metaconid apex
9	Entoconid apex
10	Hypoconulid apex

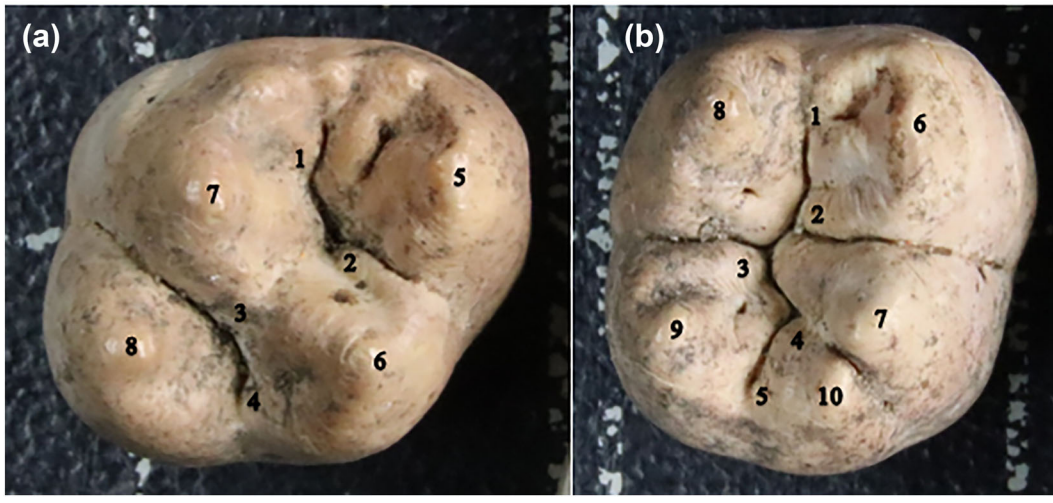

FIGURE 2 Maxillary (a) and mandibular (b) first permanent molars with numbered landmarks (see Tables 1–2 for landmark descriptions). Images orientated with mesial at the top and buccal to the right.

where k was the total number of landmarks plus semilandmarks and m the number of dimensions. As points were digitised along the x and y axes, $m = 2$. The ordering of coordinate points corresponded exactly between matrix configurations $X_1, \ldots, X_n$, and the semilandmark coordinates were stored in the top q rows of the matrix. Thus, our data consist of n coordinate matrices $X_i = (X_{ijx}, X_{ijy})^T$ where $i = 1, \ldots, n$ are the complete set of measures in a particular analysis, $j = 1, \ldots, q < k$ are semilandmark coordinates, and $j = q+1, \ldots, k$ are landmark locations.

Semilandmarks

Initially, semilandmarks were not comparable between matrix configurations as placement around each tooth's outline was done with reference to length only. There are various ways to process semilandmarks to achieve a point-to-point correspondence. For the present study, bending energy was minimised. A commonly used alternative would have been to reduce the Procrustes distance between corresponding semilandmarks in each configuration. However, in that approach, positional changes are not influenced by other landmarks or semilandmarks in the same configuration, and the final position of a semilandmark may overlap or pass that of another. In contrast, when minimising bending energy, semilandmarks "slide" along a line the length of which is restricted by the distance between points adjacent to the semilandmark; semilandmarks cannot therefore move beyond adjacent landmarks/semilandmarks from the same configuration and results more closely approximate real-world relationships (Bookstein, 1997; Gunz & Mitteroecker, 2013; Zelditch et al., 2012).

Bending energy was reduced in superimposed configurations through an iterative process. Initially, landmarks and semilandmarks were averaged to find the sample's mean shape. To align outlines more smoothly to the sample mean, semilandmarks were then slid along the line parallel to the chord connecting adjacent points (Perez et al., 2006; Zelditch et al., 2012). Thus, in configuration i, $X_i = (X_{ijx}, X_{ijy})^T$ containing q semilandmarks in positions $j = 1, \ldots, q < k$, semilandmarks are slid along tangent direction $u_j = (u_{jx}, u_{jy})^T$ with $\|u_j\| = 1$. In the resulting configuration matrix $Y_i = (Y_{ijx}, Y_{ijy})^T$, semilandmarks $j = 1, \ldots, q$ have novel positions. Landmark positions, meanwhile, are unchanged in that $Y_{ijx} = X_{ijx}$ and $Y_{ijy} = X_{ijy}$ for $j = q+1, \ldots, k$ (Bookstein, 1997; Dryden & Mardia, 2016: 368). Following this, configurations were superimposed again and the new mean shape found. The procedure was repeated until the mean shapes of successive iterations converged and it was assumed that semilandmarks from different configurations corresponded and outlines were comparable between individuals (Zelditch et al., 2012; Gunz & Mitteroecker, 2013). Note that the convention of referring to revised coordinate configurations as X_i rather than Y_i is retained as this notation is well established.

The number of semilandmarks needed to describe an outline effectively is an issue to which there is no ready answer. A balance must be achieved between undersampling, which would lead to insufficient morphological data being captured, and the loss of statistical power associated with oversampling (Dryden & Mardia, 2016: 369). In past research there has been a great deal of variability in how many semilandmarks have been used to define M1 outlines, with some projects using as few as 16 outline points and others as many as 39 (Benazzi et al., 2011; Gómez-Robles et al., 2007, 2011). Lack of standardisation is partially the result of the unique set of requirements for each study—investigators must determine how many points are appropriate to answer their specific questions (Bardua et al., 2019; Gunz & Mitteroecker, 2013; Watanabe, 2018). A random sample of the present dataset was analysed to decide how many semilandmarks to employ here. At the start of the data collection process the outlines of five antimeric M^1 and M_1 pairs were replicated five times (for a total of 50 M^1 and M_1 coordinate configurations). Outlines were then sampled by 10, 20, 30, and

40 semilandmarks. These configurations were superimposed through a generalised Procrustes analysis (GPA) and tangent plane coordinates (discussed below) were plotted through a principal components analysis (PCA) to ascertain when additional semilandmarks ceased to alter plots and presumably no longer contributed useful information to the representation of tooth morphology (Bardua et al., 2019; Watanabe, 2018). The plots from these analyses showed visually appreciable differences in configurations with 10 and 20 semilandmarks but little alteration beyond that, as illustrated for the M^1 (Figure 3). As a result, it was decided to define outlines with 20 semilandmarks. Although the decision was subjective, the number appeared to capture morphological variation in sufficient detail and provided enough points to interpret visually data in a meaningful manner whilst mitigating against the introduction of redundant information.

Procrustes superimposition

To investigate shape, it was first convenient to define and remove the effect of size. The present study used centroid size (S), which is computed as the square root of the sum of squared Euclidean distances of each coordinate point from the configuration's centre, which is found as the mean x and y coordinate (Dryden & Mardia, 2016: 34). Following this, a full generalised Procrustes analysis was carried out on the k x m x n array of coordinate configurations (landmarks and semilandmarks). To remove the nuisance parameters of scale, rotation, and translation, an iterative approach was adopted. First, locational differences were removed by translating the central points of all superimposed coordinate configurations to a common origin at (0,0). Then, the first configuration was employed as a target shape around which all other configurations were scaled and rotated through a least-squares optimisation algorithm. Following the initial fit, an average shape was computed and employed as the target for a subsequent round of fitting. This process was repeated until the average shapes produced by successive rounds ceased to differ due to the sum of squared Euclidean distances between

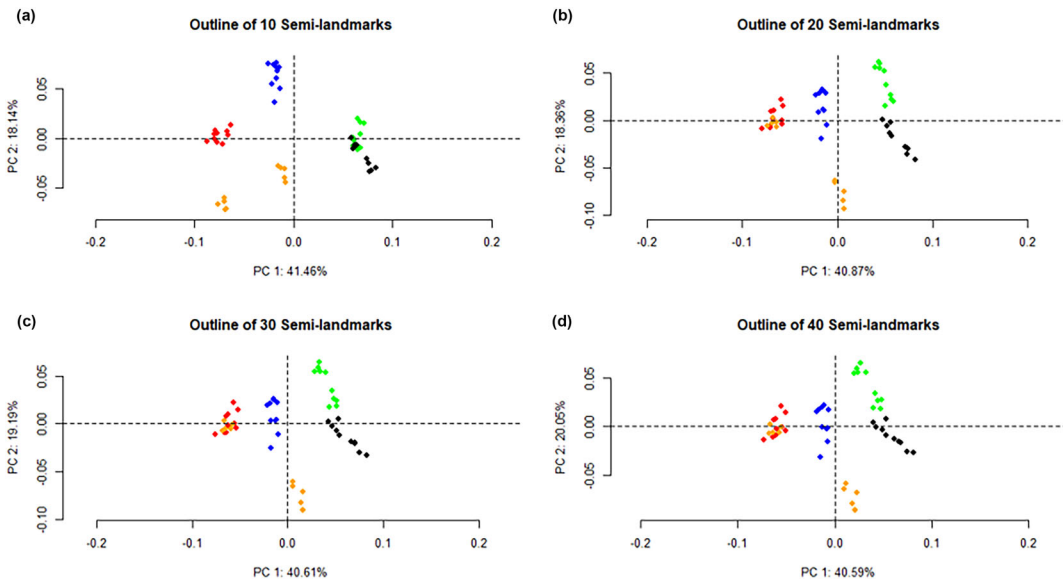

FIGURE 3 Plots of first two PCs of M^1 configurations with 10 (a), 20 (b), 30 (c), and 40 (d) semilandmarks. Colors represent five distinct individuals, each of whom is represented by five left and five right replicate configurations.

shapes $X_1,\ldots,X_n$ having been minimised (Adams et al., 2021; Dryden & Mardia, 1998; Gower, 1975; Klingenberg, 2020). The process of a full GPA thus registered configurations to a common coordinate system in Kendall's shape space by transforming them relative to one another to minimise the total sum of squares for each nuisance parameter as well as the squared full Procrustes distance (d_F^2) between configurations (Bookstein, 1991; Bookstein, 1997; Dryden & Mardia, 1998; Gower, 1975; Kendall, 1984).

To circumvent the non-Euclidean geometry of Kendall's shape space, configurations were projected into tangent linear space about a "pole"—the average shape—for inferential exploration (Dryden & Mardia, 1998; Dryden & Mardia, 2016; Kent & Mardia, 2001; Rohlf, 1999: 205). Though necessarily leading to a degree of distortion, this is negligible in most biological datasets and the Euclidean squared distances in tangent linear space (d_{υ}^2) between coordinates are amenable to standard statistical methods (Dryden & Mardia, 1998; Dryden & Mardia, 2016; Kent & Mardia, 2001; Klingenberg, 2020).

Decomposing variation

As shape differences in the tangent plane can be partitioned through a sum of squares (*SS*) procedure, with distances between configurations found as the squared differences summed across all coordinate points, variation is decomposed as

$$\sum_{p=1}^{P}\sum_{b=1}^{B} d_{\upsilon}^2\left(X_{pb},\bar{\bar{X}}\right) = B\sum_{p=1}^{P} d_{\upsilon}^2\left(\overline{X}_p,\bar{\bar{X}}\right) + P\sum_{b=1}^{B} d_{\upsilon}^2\left(\overline{X}_b,\bar{\bar{X}}\right) + \sum_{p=1}^{P}\sum_{b=1}^{B} d_{\upsilon}^2\left(X_{pb},\overline{X}_p+\overline{X}_b-\bar{\bar{X}}\right)$$

where individuals $p=1,\ldots,P$ each have sides $b=1,\ldots,B$, where $B=2$ so that X_{pb} is side b of the pth individual, $\overline{X}_p$ and $\overline{X}_b$ are individual and side means, and $\bar{\bar{X}}$ is the grand mean. The sums on the right-hand side of the equation respectively account for individual differences, directional asymmetry, and nondirectional asymmetry (i.e., antisymmetry and/or fluctuating asymmetry, as discussed below) (Savriama & Klingenberg, 2011: 5).

This decomposition was achieved through a two-way, mixed model ANOVA. This model had two main factors, a between-subjects random effect and a within-subjects fixed effect. Also accounted for was the interaction of factors and, as replicate measures were taken, variation attributable to error (Adams et al., 2021; Field, 2005; McKillup, 2012; Zelditch et al., 2012). The between-subjects effect (*ind*), or variation between individuals, was found as the sum of squared differences (i.e., squared tangent space distances) between average individual shapes (i.e., an individual's mean shape calculated from all replicate measures) and the grand mean shape (Table 3). The within-subject effect (*side*) was computed by finding the sample's average left and right-side shapes, and summing the differences between them and the grand mean shape to measure sample-level side biases attributable to directional asymmetry. The interaction between the two main effects (*ind x side*) quantified the contribution of individual left–right differences and measured nondirectional asymmetry (in simple terms, this is the variation remaining unexplained by individual differences and directional biases). Variation due to intra-observer error was calculated as the summed differences between each replicate and the corresponding individual's mean left or right configuration (Graham et al., 2010; Klingenberg, 2015; Klingenberg & McIntyre, 1998; Murrar & Brauer, 2018; Palmer & Strobeck, 1986; Zelditch & Swiderski, 2018; Zelditch et al., 2012).

The *SS* values are divided by their respective degrees of freedom to give the mean square (*MS*) for each term (Table 3), while dividing the *SS* for each effect by the total *SS* gave an R^2 value that represented the proportion of variation attributable to each term (Adams et al., 2021). To determine significance for the interaction term (i.e., nondirectional asymmetry)

TABLE 3 The ANOVA procedure through which the differences (measured as squared tangent space distances) between shapes (defined above) were computed to decompose variation. As three replicate measures were taken, $c = 1, \ldots, C$ where $C = 3$.

Effect	*SS*	*df*	*MS*
ind	$CB\sum_{p=1}^{P} d_{\upsilon}^{2}\left(\overline{X}_{p}, \bar{\bar{X}}\right)$	$P-1$	$SS_{ind}/(P-1)$
side	$CP\sum_{b=1}^{B} d_{\upsilon}^{2}\left(\overline{X}_{b}, \bar{\bar{X}}\right)$	$B-1$	$SS_{side}/(B-1)$
ind x side	$C\sum_{p=1}^{P}\sum_{b=1}^{B} d_{\upsilon}^{2}\left(\overline{X}_{pb}, \left(\overline{X}_{p}+\overline{X}_{b}-\bar{\bar{X}}\right)\right)$	$(P-1)(B-1)$	$SS_{ind\ x\ side}/(P-1)(B-1)$
error	$\sum_{c=1}^{C}\sum_{p=1}^{P}\sum_{b=1}^{B} d_{\upsilon}^{2}(X_{pbc}, \overline{X}_{pb})$	$PB(C-1)$	$SS_{error}/PB(C-1)$
Total	$\sum_{c=1}^{C}\sum_{p=1}^{P}\sum_{b=1}^{B} d_{\upsilon}^{2}\left(X_{pbc}, \bar{\bar{X}}\right)$	$PBC-1$	

an F-value was computed as $F = MS_{ind\times side}/MS_{error}$ (Graham et al., 2010; Klingenberg, 2015; Klingenberg & McIntyre, 1998; Zelditch & Swiderski, 2018; Zelditch et al., 2012). To avoid the need to make normality assumptions, significance testing was done nonparametrically through a residual randomization permutation procedure (RRPP) (Collyer, 2015; Collyer et al., 2015; Edgington, 1995; Good, 1994; Graham et al., 2010: 487–489; Klingenberg, 2015; Klingenberg & McIntyre, 1998). In RRPP, residuals from null linear models are randomized and added to the fitted values to generate random pseudovalues from which pseudo-ANOVA statistics are drawn. By doing this repeatedly, an empirical sampling distribution of ANOVA statistics is produced (Adams & Collyer, 2015; Anderson & Ter Braak, 2003; Collyer & Adams, 2018; Zelditch et al., 2012). Thus, the F-values for the observed effects were compared to the distribution of many values and deemed significant when they fall beyond the 95th percentile.

Contingent upon significant results, coordinate configurations were investigated further to discern whether the nondirectional component to asymmetry was likely the result of random deviations from symmetry (i.e., was the interaction term identifying significant fluctuating asymmetry). Consequently, for each M1 landmark and semilandmark plots of signed left–right differences were visually examined and tested for kurtosis; if antisymmetry was present, scatter plots would reveal two clusters, whereas histograms and density plots would display a bimodal or platykurtic distribution (Balzeau et al., 2012; Debat et al., 2000; Guatelli-Steinberg et al., 2006; Klingenberg & McIntyre, 1998; Radwan et al., 2003; Silva et al., 2012).

Individual measure

Assuming the nondirectional component to asymmetry was identified as fluctuating asymmetry rather than antisymmetry, configurations were further transformed to isolate the directional and fluctuating components to asymmetry. When handling x-y coordinate configurations, the directional component to asymmetry (D) is computed as the difference between the overall sample's mean left $(\overline{x\text{-}y})_L$ and right $(\overline{x\text{-}y})_R$ configuration (Bookstein, 1991; Klingenberg & McIntyre, 1998; Oxilia et al., 2021; Palmer & Strobeck, 2003; Smith et al., 1997; Zelditch et al., 2012). The k x m matrix D is given as

$$\mathrm{D} = (\overline{\mathrm{x\text{-}y}})_{\mathrm{L}} - (\overline{\mathrm{x\text{-}y}})_{\mathrm{R}}.$$

By subtracting the directionally asymmetric component to asymmetry (D) from the difference between the individual left $(x\text{-}y)_L$ and right $(x\text{-}y)_R$ coordinate configurations (as repeated measures were taken, here individual left and right configurations are replicate averages), it is possible to obtain a k x m matrix of x-y coordinates for individuals $p = 1, \ldots, P$ that reflects the component of morphological variation attributable to fluctuating asymmetry (Adams et al., 2021; D. Adams, personal communication, May 21, 2020). For the pth individual this is calculated as

$$A_p = \left((x\text{-}y)_{pL} - (x\text{-}y)_{pR}\right) - D.$$

To calculate a univariate index of fluctuating asymmetry (a_p), from A_p configurations the square root of the sum of squares is found to give.

$$a_p = \sqrt{\sum_{i=1}^{k}\sum_{j=1}^{m}(A_{pij})^2}.$$

As an unsigned individual estimate of the magnitude of M1 fluctuating asymmetry, a_p scores are amenable to standard univariate tests and can be employed to explore differences in the intensity of early-life stress (Bookstein, 1991; Klingenberg & McIntyre, 1998; Lazić et al., 2015; Oxilia et al., 2021; Palmer, 1994; Palmer & Strobeck, 2003; Smith et al., 1997; Zelditch et al., 2012). The data generated by these procedures were stored in ORDA, the University of Sheffield's data repository, and can be found at: https://doi.org/10.15131/shef.data.25348111.v2. A description of the project's workflow and reproducible code are supplied in APPENDIX S1: DATA ACQUISITION AND ANALYSIS.

RESULTS

Procrustes ANOVA

The Procrustes ANOVA indicated that the greatest proportion of variation (circa 83%) in both M1s was explained by individual differences (Tables 4–5). Despite the majority of variation not being explained by asymmetry, significant sample-level left–right differences (i.e., directional asymmetry) were detected in both the M^1 ($p = 0.003$) and M_1 ($p = 0.008$); these accounted for only a minor percentage of total morphological variation (i.e., 0.2%–0.3%), however. Highly significant interactions ($p = 0.001$) between individuals and sides revealed the presence of non-directional asymmetry. Importantly, differences between replicates (i.e., error due to intra-

TABLE 4 M^1 Procrustes ANOVA. Significance determined through RRPP with 1,000 permutations.

Effects	df	SS	MS	R^2	F	p
ind	153	3.530	0.023	0.833	5.854	0.781
side	1	0.011	0.011	0.002	2.862	0.003
ind x side	153	0.603	0.004	0.142	26.411	0.001
error	616	0.091	<0.001	0.021		
Total	923	4.237				

TABLE 5 M_1 Procrustes ANOVA. Significance determined through RRPP with 1,000 permutations.

Effects	Df	SS	MS	R^2	F	p
ind	147	4.507	0.031	0.826	5.362	0.977
side	1	0.014	0.014	0.003	2.406	0.008
ind x side	147	0.841	0.006	0.154	36.107	0.001
error	592	0.094	<0.001	0.017		
Total	887	5.455				

observer inconsistency) accounted for a small percentage of overall variation (circa 2%) in both M1s. In fact, F values indicated that M^1 nondirectional asymmetry explained in excess of 26 times more variation than error ($F = 26.411$); for the M_1 this increased to greater than 36 times ($F = 36.107$). Crucially, when the signed left–right differences for each landmark and semilandmark were examined, evidence of antisymmetry was absent (i.e., there was no clustering in scatter plots, whereas histograms and density plots revealed highly peaked rather than platykurtic distributions). This is consistent with previous research, which has not found antisymmetry in human teeth (e.g., Guatelli-Steinberg et al., 2006). It was therefore inferred that the nondirectional component to asymmetry was in fact fluctuating asymmetry, with R^2 values implying that stress-induced deviations from perfect symmetry made a moderate contribution to morphological variation (circa 14%–15%).

Adjusted configurations

A_p configurations were examined to explore the locations at which stress-induced phenotypic errors were most evident. When the complex patterns in coordinates matrices were simplified through PCA, variation was found to be dispersed throughout configurations; for example, it took 15 and 19 PCs to capture ≥95% of variation in the M^1 and M_1 covariance matrices respectively. The first two PCs were, however, influenced to a greater extent by semilandmarks located along the outline and landmarks positioned at fissure junctions and pits (i.e., points at the periphery of cusps). The eigenvectors of the third and fourth PCs, by contrast, had higher loadings on cusp apices, especially those of the distal cusps. Meanwhile, the mesial cusps (paracone and protocone in the M^1 and the protoconid and metaconid in the M_1) were relatively stable. These patterns are best appreciated visually; therefore, the configurations with the most extreme differences in each PC were plotted and vector displacements compared (Figure 4). These procedures suggested that fluctuating asymmetry predominantly manifested at the edges of cusps, and that when cusps apices did vary, the distal cusps were more likely to be affected than the mesial. Potentially, these findings could lead into further research relating to the physiological mechanisms underlying M1 occlusal FA and developmental modularity/integration in multicusped teeth.

Individual scores

When unsigned univariate FA scores (i.e., a_p values) were inspected, density and quantile-quantile plots indicated peaked or "light-tailed" and positively skewed distributions, potentially influenced by outlying values (Table 6 and Figure 5). Plots also revealed a second, smaller peak within the right tail of each distribution, suggesting the presence of two distinct groups within the sample. It was further noted that, due to the arbitrary nature of the registration process, M1

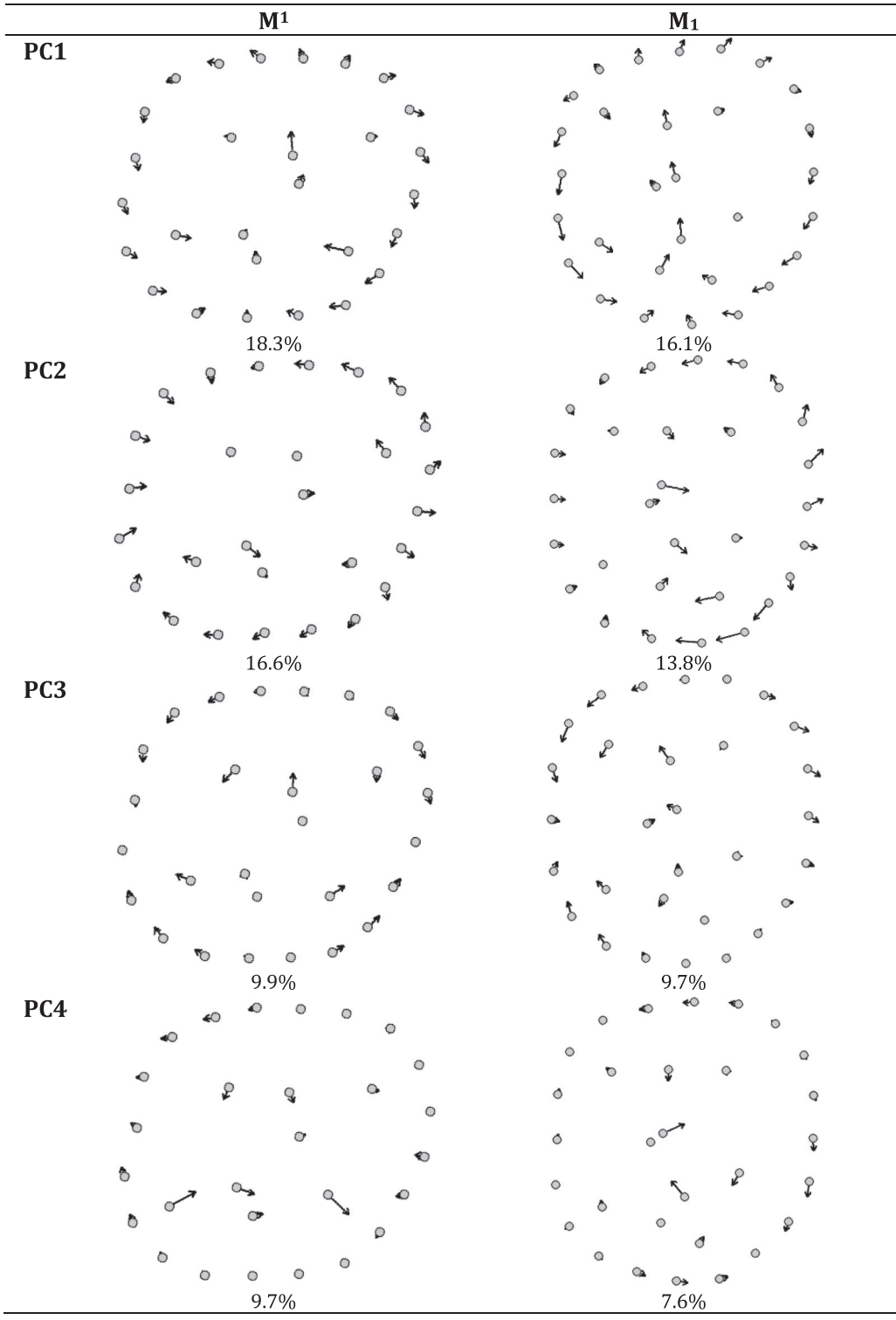

FIGURE 4 Vector displacements (length and orientation of line indicate magnitude and direction) between reference and target shapes (i.e., teeth contributing the least and most variation) in the first four PCs. Percentages correspond to the proportion of variation accounted for by each PC. Mesial is up.

TABLE 6 A summary of M1 a_p scores (before log transformation and scaling).

Tooth	No.	Min	Q1	Median	Mean	Q3	Max	Std dev
M^1	154	1.000369	1.000790	1.001176	1.001304	1.001776	1.003410	0.000678
M_1	148	1.000477	1.001253	1.001738	1.001891	1.002566	1.003846	0.000812

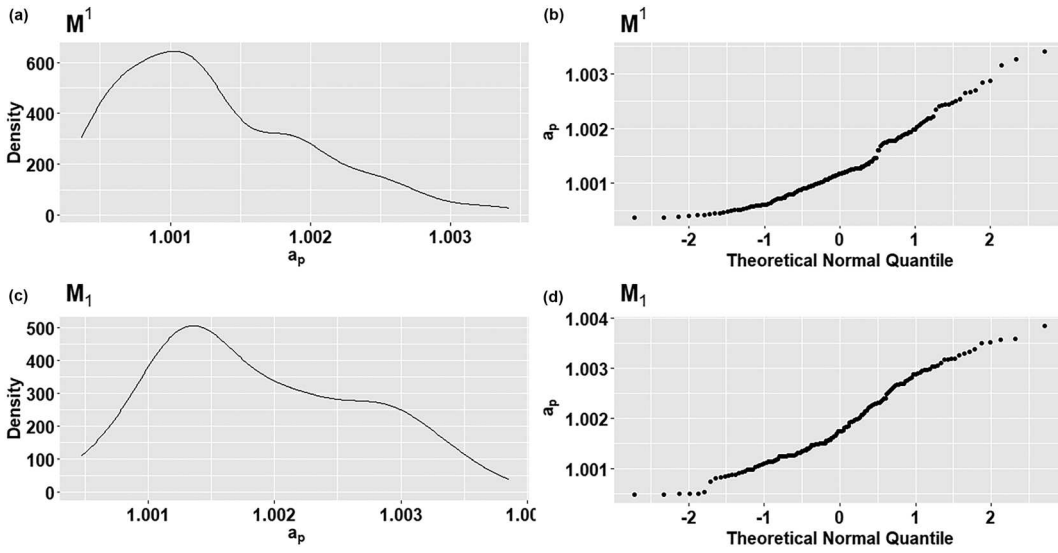

FIGURE 5 Density and quantile–quantile plots of M^1 (a–b) and M_1 a_p scores (c–d).

a_p scores were expressed on a small scale (Dryden & Mardia, 1998; Zelditch & Swiderski, 2018). These distributional and scaling characteristics required consideration, and it was decided that when subjecting M1 a_p scores to quantitative procedures, the scaled natural logarithm would be used. After logarithmic transformation, scores better approximated a normal distribution (Van Pool & Leonard, 2010). Meanwhile, scaling mitigated against the computational difficulties associated with exploring small differences (Grus, 2015). To scale scores, the sample mean was subtracted from each individual a_p value to centre them, then centred scores were divided by the sample's standard deviation (Grus, 2015). These transformations facilitated statistical testing.

To investigate potential influences of size on FA, the relationship between a_p scores and the left–right difference of centroid size was explored (Klingenberg, 2015; Klingenberg & McIntyre, 1998). Regression tests found no significant relationship between either transformed M^1 ($F[1,152] = 1.436$, $p = 0.233$) or M_1 a_p scores ($F[1,146] = 1.034$, $p = 0.319$) and size asymmetry. However, among the 85 individuals for whom both maxillary and mandibular M1s could be assessed, linear regression found that transformed M_1 a_p scores could be used to predict the corresponding M^1 value ($F[1,83] = 15.57$, $p = <0.001$, $R^2 = 0.148$). Although the R^2 value associated with the model indicated only a moderate proportion of variation had been explained, the result implied a connection between the processes that led to stress-induced deviations to symmetry in each isomere and that M^1 and M_1 a_p scores likely reflected the same underlying causal factors.

Bioarchaeological application

To demonstrate the utility of the protocol in bioarchaeological investigations, universally relevant comparisons were made. Specifically, transformed M1 a_p scores were contrasted between sites, sexes, as well as skeletally mature and immature cohorts. This exploration of M1 a_p scores revealed subtle differences between sites in FA (Figure 6a,b). Insignificant Levene's tests suggested between-group variance was comparable in M^1 ($F[3,149] = 2.62$, $p = 0.053$) and M_1 a_p scores ($F[3,144] = 0.897$, $p = 0.444$), justifying parametric testing. An ANOVA found significant differences between sites in transformed M^1 a_p scores ($F[3,149] = 7.703$, $p = <0.001$) with moderate effect size ($\omega^2 = 0.12$). *Post-hoc* pairwise comparisons with Bonferroni-adjusted thresholds inferred significant differences ($p < 0.05$) between the Warwick assemblage and the other three sites. Between-site differences in M_1 a_p scores were, however, insignificant ($F[3,144] = 0.776$, $p = 0.509$). Moreover, no significant differences were discernible between females and males in transformed M^1 ($t = -0.600$, $df = 55.98$, $p = 0.551$) or M_1 a_p scores ($t = -1.399$, $df = 57.75$, $p = 0.167$) (Figure 6c,d). From these results it was inferred that between-site differences in early-life stress were either relatively slight or that a buffering mechanism had mediated site-specific stressors, and that sex differentials in early-life stress resilience were not apparent. In contrast, when a_p scores were compared between skeletally mature and immature individuals, it was observed that the immature cohort had higher scores for both M1s (Figure 6e,f). After removing the outlying datapoint from the skeletally mature group, a *t*-test with Welch's correction on transformed M^1 scores produced significant results ($t = 5.202$, $df = 128.4$, $p = <0.001$) with large effect size (Cohen's $d = -0.848$). Similarly, differences in M_1 a_p scores were significant ($t = 3.159$, $df = 136.1$, $p = 0.002$) with a medium effect size (Cohen's $d = -0.526$). It therefore appeared that variation in early-life stress affected mortality risk and skeletal development.

DISCUSSION

A Procrustes ANOVA revealed that the largest percentage of M1 morphological variability was accounted for by individual differences. Directional biases only constituted a small proportion of variation in comparison to nondirectional asymmetry. Meanwhile, comparing signed left–right differences at specific landmarks and semilandmarks revealed peaked distributions, suggesting the nondirectional biases identified through the interaction term of the ANOVA procedure represented random, stress-induced deviations to perfect symmetry rather than a predisposition for one side to be consistently different from the other. In other words, the process successfully detected significant levels of fluctuating asymmetry. Importantly, differences between replicates were minor, with *F* ratios indicating intra-observer error was sufficiently small (circa 2% of variation) that it is unlikely to interfere with analyses of FA. For future application, however, inter-observer reliability is worth considering as analyses to FA are highly sensitive to error and previous research has yielded varying results (Graham et al., 2010; Klingenberg, 2015). For example, although Kenyhercz et al. (2014) found no significant observer differences in M1 occlusal landmark positioning, Robinson et al. (2002) suggested that inter-observer error accounted for >50% of M1 morphological variation in their dataset. Likely these disparities relate to training and observer experience and the impact this has on the ability to replicate precisely a multistage data collection process (Robinson et al., 2002; Shearer et al., 2017). It is therefore recommended that when reproducing the method presented here, in addition to taking replicate measures, a period of familiarisation training is undertaken and that either one observer generates all data or, if multiple observes are employed, calibration testing is conducted. Under these conditions, the protocol can be applied consistently to produce highly accurate results.

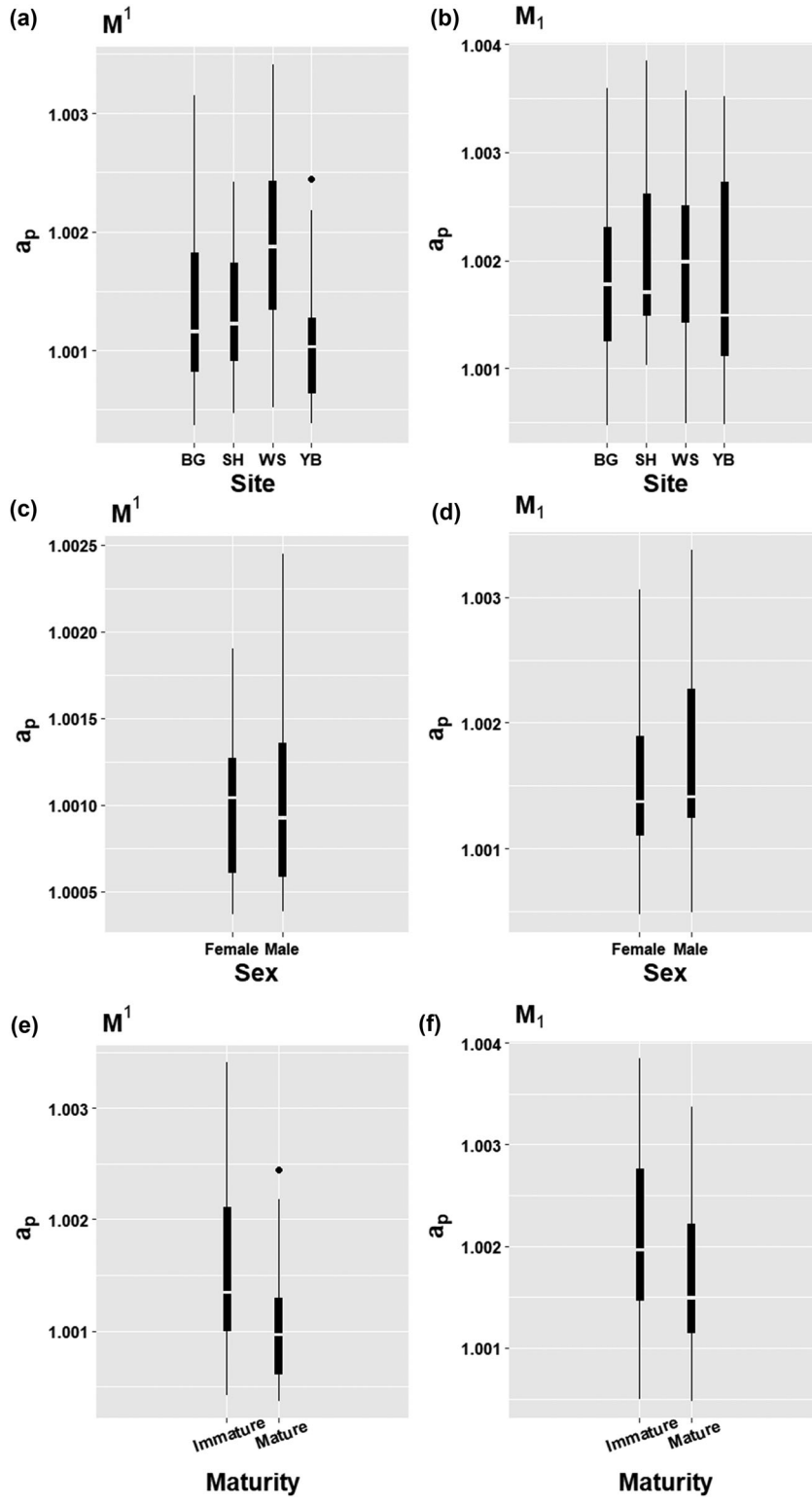

FIGURE 6 M^1 and M_1 a_p scores contrasted between the Black Gate (BG), South Shields (SH), Warwick (WS), and York Barbican (YB) sites (a-b) as well as sexes (c–d) and skeletally mature and immature groups (e–f).

It could be argued that morphological information was lost in the "flattening" of three-dimensional objects into two-dimensional coordinate configurations (Klingenberg, 2015: 889). However, comparisons of two- and three-dimensional procedures generally find similar results, with differences only apparent where variability is predominantly located along the third axis (e.g., Buser et al., 2018; Wasiljew et al., 2020). Given cusp height is dependent on and can be predicted by, its distances from other cusps (Hunter et al., 2010; Jernvall 2000; Jernvall & Jung, 2000), it is unlikely that information contained along the additional third axis would contribute novel information regarding M1 occlusal morphology. Moreover, sampling from teeth sufficiently unworn for the height/depth of features to be assessed would greatly reduce sample size in an archaeological context. By contrast, a two-dimensional protocol was more accommodating in that, although moderately-to-heavily worn M1s had to be excluded, it was possible to include teeth when minor wear had only slightly affected cusp apices and the position of these points could be estimated from exposed patches of dentine (Gómez-Robles et al., 2007; Kenyhercz et al., 2014). The requirement for reasonably well-preserved teeth undoubtedly constrains the method's application in certain respects (e.g., assessment of prehistoric populations with abrasive diets would be difficult). However, it is well suited to other analyses. For example, postmedieval groups can be assessed more easily due to their refined diets (Raynor et al., 2011: 55). Younger and skeletally immature individuals, in addition to being a highly informative cohort from a palaeopathological and epidemiological standpoint, will also be more amenable to the method presented here (Gowland, 2015; Hodson & Gowland, 2020; Lewis, 2017). Moreover, in a different setting, if desired and the absence of dental wear makes it appropriate, the protocol could be modified easily to produce three-dimensional data.

Importantly, the method produces novel and informative findings. To illustrate, by contrasting the A_p configurations that contributed the greatest and least variation to PCs, interesting patterns regarding the distribution of stress-induced deviations away from target phenotype in M1s were revealed. As phenotypic errors were more likely to occur at the edges of cusps, it is suggested that cusp development is relatively stable—especially for mesial cusp apices that appeared to be least affected by developmental stressors. This is consistent with the patterning cascade model (PCM) of tooth development. The PCM posits that in multicusped teeth the relationships between occlusal features are determined by biomolecular feedback loops centred around developing cusp apices and involving several gene families that can either promote or perturb growth depending on how they interact (Jernvall & Jung, 2000; Salazar-Ciudad & Jernvall, 2002). It has been proposed this developmental mechanism is stress sensitive and that stressors can disrupt the layers of iterative reactions, which are initially focused around the early developing mesial cusps, increasing developmental errors in later-forming features (i.e., those on the periphery of cusps or distal cusps). Although past research has supported this hypothesis, finding that groups with evidence of stress also had a higher frequency of occlusal polymorphisms and greater variability in the expression of additive traits (Hunter et al., 2010; Riga et al., 2014; Townsend et al., 2003), by taking a GM approach it was possible to model the relationships more clearly between occlusal features. It is therefore suggested that FA, quantified through the methods detailed here, can be employed to investigate retrospectively in vivo developmental processes, and it is proposed that further work can be done to explore themes such as developmental modularity versus integration. As such, the protocols described in this paper have the capacity to be useful interrogative tools not only in the field of bioarchaeology but also disciplines such as zooarchaeology, palaeoanthropology, and palaeontology.

The results of this study also suggest that the unsigned individual index of M1 FA (a_p scores) is a useful metric through which to investigate and compare the intensity of early-life stress experienced within and between groups. It had initially been wondered if an allometric effect would complicate analyses. That is, as size increases, the maintenance of developmental stability becomes more difficult and larger structures can exhibit higher FA by virtue of their scale. However, as left–right differences in centroid size did not predict M1 a_p scores, it seems

unlikely that allometry confounded analyses (Klingenberg, 2015; Klingenberg & McIntyre, 1998). Moreover, as M_1 a_p scores were significant (if weak) predictors of corresponding M^1 a_p values ($F[1,83] = 15.57$, $p = <0.001$, $R^2 = 0.148$), it appears that the morphological variability noted in each isomere was influenced by the same underlying factor. Simply put, this supports the assumption that FA can be used as a proxy for nonspecific physiological stress, and, as such, potentially M^1 and M_1 a_p scores could be aggregated into a composite FA score, which should in theory provide a more robust estimate of developmental stress (Graham & Ozener, 2016; Klingenberg, 2015; Palmer & Strobeck, 2003).

It was, however, surprising that differences in scores between sites, which varied substantially in terms of temporal and sociocultural context, were relatively subtle and well-established sex biases in frailty were absent (DeWitte, 2010; Mahoney Swales, 2019; Raynor et al., 2011). This may, however, be related to the fact that M1s develop whilst offspring are maternally dependent. It is speculated that maternal buffering mitigated contextual stressors and biological differences in vulnerability. This aligns well with previous investigations that have found significant differences in FA between sites and sexes for most teeth (e.g., Barrett et al., 2012; Guatelli-Steinberg et al., 2006; Townsend & Brown, 1980), with the M1 and deciduous dentition (which also form whilst maternally dependent) being a frequent exception (e.g., Noss et al., 1983; Townsend, 1981). Moreover, the observation that skeletally immature individuals had significantly higher M^1 ($t = 5.202$, df = 128.4, $p = <0.001$, Cohen's $d = -0.848$) and M_1 a_p scores ($t = 3.159$, df = 136.1, $p = 0.002$, Cohen's $d = -0.526$) with medium-to-large effect size is consistent with clinical and bioarchaeological research, which has implicated maternally mediated, early-life stress in developmental delays and differentials in morbidity and mortality (Barker, 2012; Gowland, 2015; Roseboom et al., 2001). This suggests that future bioarchaeological research adopting a life-course approach will be particularly productive. Specifically, M1 a_p scores in conjunction with later-forming skeletal stress markers (e.g., linear enamel hypoplasia, cribra orbitalia, periosteal new bone formation) could be employed to chart stress experience across the life course and explore the impact of perturbations experienced at critical phases of life alongside themes such as maternal buffering and environmental stress.

The GM protocols presented here, in which complex morphology is defined through x-y coordinates at anatomical landmarks and an outline of semilandmarks, have been shown to be a sensitive means of detecting and decomposing asymmetrical variation. The method is nondestructive, flexible enough to accommodate practical challenges (e.g., dental wear), and can be accomplished with minimal intra-observer replication error using widely accessible equipment in conjunction with freely available software (Adams et al., 2021; Olsen, 2015; Zelditch & Swiderski, 2018). In sum, this protocol is highly repeatable and not limited to the bioarchaeological analysis of dental FA but could be applied to any bilateral structure. We therefore conclude that this approach can be employed to address a range of research questions, shed light on in vivo ontogenetic processes and provide a means through which the otherwise invisible imprints of developmental stress can be reconstructed.

CONCLUSION

This paper has detailed a statistically rigorous method through which developmental stress can be reconstructed. Through a bioarchaeological case study, it was demonstrated that the Procrustes ANOVA model permits tangent space distances to be decomposed so that phenotypic variation can be explored and which is sensitive to the small stress-induced developmental errors that characterise fluctuating asymmetry—this represents a significant improvement on traditional measures and methods (Adams et al., 2021; Dryden & Mardia, 1998; Klingenberg & McIntyre, 1998; Zelditch et al., 2012). Moreover, the processing of coordinate configurations to isolate FA enabled the locations in which phenotypic variation was concentrated on the

occlusal surface of M1s to be identified and the intensity of stress experience to be contrasted between groups. It was therefore possible to comment on and empirically support the patterning cascade model, which purports to explain the development of multicusped teeth and also infer that early-life stress played a critical role in mortality risk and development, but that mothers likely mitigated sex differentials in frailty and the impact of site-specific stressors. From this it is proposed that further work could be done to investigate developmental modularity and integration in dental morphology and that a bioarchaeological project collating data on early and later-forming stress markers could explore the possible interactions of experiences over the life course. More broadly, these findings illustrate that FA and its interrogation through GM protocols have the capacity to illuminate in vivo developmental processes and the intensity of stress experience, and it is anticipated that these methods can be employed in a range of fields to investigate a diverse spectrum of research questions.

DATA AVAILABILITY STATEMENT

The data that support the findings of this study are openly available in ORDA at https://orda.shef.ac.uk/.

ORCID

Ben Wigley https://orcid.org/0000-0003-1188-342X
Eleanor Stillman https://orcid.org/0000-0002-5971-0985
Elizabeth Craig-Atkins https://orcid.org/0000-0003-2560-548X

REFERENCES

Adams, D. C., Collyer, M. L., Kaliontzopoulou, A., & Baken, E. (2021). *Geomorph: Software for geometric morphometric analyses*. R Package Version 4.0.0. https://cran.r-project.org/package=geomorph

Adams, D. C., Rohlf, F. J., & Slice, D. E. (2004). Geometric morphometrics: Ten years of progress following the "revolution.". *Italian Journal of Zoology*, *71*(1), 5–16. https://doi.org/10.1080/11250000409356545

Anderson, M. J., & Ter Braak, C. J. F. (2003). Permutation tests for multifactorial analysis of variance. *Journal of Statistical Computation and Simulation*, *73*(2), 85–113. https://doi.org/10.1080/00949650215733

Antoine, D., & Hillson, S. (2016). Enamel Structure and Properties. In J. D. Irish & G. R. Scott (Eds.), *A companion to dental anthropology* (First ed.) (pp. 223–243). Wiley.

Armelagos, G. J., Goodman, A. H., Harper, K. N., & Blakey, M. L. (2009). Enamel hypoplasia and early mortality: Bioarchaeological support for the Barker hypothesis. *Evolutionary Anthropology*, *18*, 261–271. https://doi.org/10.1002/evan.20239

Bailit, H., Workman, P., Niswander, J., & MacLean, C. (1970). Dental asymmetry as an Indicator of genetic and environmental conditions in human populations. *Human Biology*, *42*(4), 626–638.

Balzeau, A., Gilissen, E., & Grimaud-Herve, D. (2012). Shared pattern of endocranial shape asymmetries among great apes, anatomically modern humans, and fossil hominins. *PLoS ONE*, *7*(1), e29581. https://doi.org/10.1371/journal.pone.0029581

Bardua, C., Felice, R. N., Watanabe, A., Fabre, A.-C., & Goswami, A. (2019). A practical guide to sliding and surface semilandmarks in morphometric analyses. *Integrative Organismal Biology*, *1*(1), 1–34. https://doi.org/10.1093/iob/obz016

Barker, D. J. P. (2012). The developmental origins of health and disease. *Public Health*, *126*, 186–189. https://doi.org/10.1016/j.puhe.2011.11.014

Barrett, C. K., Guatelli-Steinberg, D., & Sciulli, P. W. (2012). Revisiting dental fluctuating asymmetry in Neandertals and modern humans. *American Journal of Physical Anthropology*, *149*(2), 193–204. https://doi.org/10.1002/ajpa.22107

Benazzi, S., Coquerelle, M., Fiorenza, L., Bookstein, F., Katina, S., & Kullmer, O. (2011). Comparison of dental measurement systems for taxonomic assignment of first molars. *American Journal of Physical Anthropology*, *144*, 342–354. https://doi.org/10.1002/ajpa.21409

Betts, J. G., Desaix, P., Johnson, E., Korol, O., Kruse, D., Poe, B., Wise, J. A., Womble, M., & Young, K. A. (2017). *Anatomy and physiology*. Rice University Press.

Bookstein, F. L. (1991). *Morphometric tools for landmark data. Geometry and biology*. Cambridge University Press. https://doi.org/10.1017/CBO9780511573064

Bookstein, F. L. (1997). Landmark methods for forms without landmarks: Localizing group differences in outline shape. *Medical Image Analysis*, *1*, 225–243. https://doi.org/10.1016/S1361-8415(97)85012-8

Brickley, M. B. (2018). Cribra orbitalia and porotic hyperostosis: A biological approach to diagnosis. *American Journal of Physical Anthropology*, *167*, 896–902. https://doi.org/10.1002/ajpa.23701

Brickley, M. B., Kahlon, B., & D'Ortenzio, L. (2020). Using teeth as tools: Investigating the mother–infant dyad and developmental origins of health and disease hypothesis using vitamin D deficiency. *American Journal of Physical Anthropology*, *171*, 342–353. https://doi.org/10.1002/ajpa.23947

Briggs, A. W., Stenzel, U., Meyer, M., Krause, J., Kircher, M., & Pääbo, S. (2010). Removal of deaminated cytosines and detection of in vivo methylation in ancient DNA. *Nucleic Acids Research*, *38*, e87. https://doi.org/10.1093/nar/gkp1163

Buikstra J. E. & Ubelaker D. H. (1994). Standards for data collection from human skeletal remains. Arkansas: Twelfth Printing 2010.

Buser, T. J., Sidlauskas, B. L., & Summers, A. P. (2018). 2D or not 2D? Testing the utility of 2D vs. 3D landmark data in geometric morphometrics of the sculpin subfamily Oligocottinae (*Pisces; Cottoidea*). *Anatomical Record*, *301*, 806–818. https://doi.org/10.1002/ar.23752

Cao-Lei, L., Massart, R., Suderman, M. J., Machnes, Z., Elgbeili, G., Laplante, D. P., Szyf, M., & King, S. (2014). DNA methylation signatures triggered by prenatal maternal stress exposure to a natural disaster: Project ice storm. *PLoS ONE*, *9*(9), e107653. https://doi.org/10.1371/journal.pone.0107653

Collyer, M. L. (2015). ANOVAs and geomorph. [online] R-bloggers. [Viewed 31st August 2020]. Available from: https://www.r-bloggers.com/anovas-and-geomorph/

Collyer, M. L., & Adams, D. C. (2018). RRPP: An R package for fitting linear models tohigh-dimensional data using residual randomization. *Methods in Ecology Evolution 9*, 1772–1779.

Collyer, M. L., Sekora, D. J., & Adams, D. C. (2015). A method for analysis of phenotypic change for phenotypes described by high-dimensional data. *Heredity*, *115*(4), 357–365. https://doi.org/10.1038/hdy.2014.75

Cucchi, T., Hulme-Beaman, A., Yuan, J., & Dobney, K. (2011). Early Neolithic pig domestication at Jiahu, Henan Province, China: Clues from molar shape analyses using geometric morphometric approaches. *Journal of Archaeological Science*, *38*(1), 11–22. https://doi.org/10.1016/j.jas.2010.07.024

Debat, V., Alibert, P., David, P., Paradis, E., & Auffray, J.-C. (2000). Independence between developmental stability and canalization in the skull of the house mouse. *Proceedings of the Royal Society Biological Sciences*, *267*(1442), 423–430. https://doi.org/10.1098/rspb.2000.1017

DeWitte, S. N. (2010). Sex differentials in frailty in Medieval England. *American Journal of Physical Anthropology*, *143*(2), 285–297. https://doi.org/10.1002/ajpa.21316

DeWitte, S. N., & Stojanowski, C. (2015). The osteological paradox 20 years later: Past perspectives, future directions. *Journal of Archaeological Research*, *23*, 397–450. https://doi.org/10.1007/s10814-015-9084-1

DeWitte, S. N., & Wood, J. W. (2008). Selectivity of black death mortality with respect to preexisting health. *Proceedings of the National Academy of Science*, *105*(5), 1436–1441. https://doi.org/10.1073/pnas.0705460105

Dryden, I. L., & Mardia, K. V. (1998). *Statistical shape analysis*. Wiley.

Dryden, I. L., & Mardia, K. V. (2016). *Statistical shape analysis, with applications in R* (Second ed.). Wiley. https://doi.org/10.1002/9781119072492

Dukić, Z. (2014). Depth of field in dental photography and methods for its control. *Serbian Dental Journal*, *61*(3), 149–156. https://doi.org/10.2298/SGS1403149D

D'Urso, A., & Brickner, J. H. (2014). Mechanisms of epigenetic memory. *Trends in Genetics*, *30*(6), 230–236. https://doi.org/10.1016/j.tig.2014.04.004

Edgington, E. S. (1995). *Randomization tests*. Marcel Dekker.

Edwards, P. D., & Boonstra, R. (2018). Glucocorticoids and CBG during pregnancy in mammals: Diversity, pattern, and function. *General and Comparative Endocrinology*, *259*, 122–130. https://doi.org/10.1016/j.ygcen.2017.11.012

Escós, J. M., Alados, C. L., Pugnaire, F. I., Puigdefábregas, J., & Emlen, J. M. (2000). Stress resistance strategy in arid land shrub: Interaction between developmental instability and fractal dimension. *Journal of Arid Environments*, *45*, 325–336. https://doi.org/10.1006/jare.2000.0641

Ferembach, D., Schwidetzky, I., & Stloukal, M. (1980). Recommendations for age and sex diagnoses of skeletons. *Journal of Human Evolution*, *9*, 517–549. https://doi.org/10.1016/0047-2484(80)90061-5

Field, A. (2005). *Discovering statistics using SPSS* (Second ed.). SAGE Publications Ltd.. https://doi.org/10.53841/bpspag.2005.1.56.31

Gómez-Robles, A., Martinon-Torres, M., Bermudez de Castro, J. M., Prado, L., Sarmiento, S., & Luis Arsuaga, J. (2008). Geometric morphometric analysis of the crown morphology of the lower first premolar of hominins, with special attention to Pleistocene Homo. *Journal of Human Evolution*, *55*(4), 627–638. https://doi.org/10.1016/j.jhevol.2008.03.011

Gómez-Robles, A., Martinon-Torres, M., de Castro, J. M. B., Margvelashvili, A., Batir, M., Arsuaga, J. L., & Martinez, L. M. (2007). A geometric morphometric analysis of hominin upper first molar shape. *Journal of Human Evolution*, *53*(3), 272–285. https://doi.org/10.1016/j.jhevol.2007.02.002

Gómez-Robles, A., Olejniczak, A. J., Martinón-Torres, M., Prado-Simón, L., & Bermúdez de Castro, J. M. (2011). Evolutionary novelties and losses in geometric morphometrics: A practical approach through hominin molar morphology. *Evolution*, *65*(6), 1772–1790. https://doi.org/10.1111/j.1558-5646.2011.01244.x

Good, P. (1994). *Permutation tests: A practical guide to resampling methods for testing hypotheses*. Springer-Verlag. https://doi.org/10.1007/978-1-4757-2346-5

Gower, J. C. (1975). Generalized Procrustes analysis. *Psychometrika*, *40*(1), 33–51. https://doi.org/10.1007/BF02291478

Gowland, R. L. (2015). Entangled lives: Implications of the developmental origins of health and disease hypothesis for bioarchaeology and the life course. *American Journal of Physical Anthropology*, *158*, 530–540. https://doi.org/10.1002/ajpa.22820

Graham, J. H., & Ozener, B. (2016). Fluctuating asymmetry of human populations: A review. *Symmetry*, *8*, 154. https://doi.org/10.3390/sym8120154

Graham, J. H., Raz, S., Hagit, H., & Nevo, E. (2010). Fluctuating asymmetry: Methods, theory and applications. *Symmetry*, *2*, 466–495. https://doi.org/10.3390/sym2020466

Green, R. E., Briggs, A. W., Krause, J., Prufer, K., Burbano, H. A., Siebauer, M., Lachmann, M., & Pääbo, S. (2009). The Neandertal genome and ancient DNA authenticity. *European Molecular Biology Organization Journal*, *28*, 2494–2502. https://doi.org/10.1038/emboj.2009.222

Grus, J. (2015). *Data science from scratch first principles with Python*. O'Reilly.

Guatelli-Steinberg, D., Sciulli, P., & Edgar, H. J. H. (2006). Dental fluctuating asymmetry in the Gullah: Tests of hypotheses regarding developmental stability in deciduous vs permanent teeth. *American Journal of Physical Anthropology*, *129*, 427–434. https://doi.org/10.1002/ajpa.20237

Gunz, P., & Mitteroecker, P. (2013). Semilandmarks: A method for quantifying curves and surface. *Hystrix*, *24*(1), 103–109.

Harris, E. F. (2016). Odontogenesis. In J. D. Irish & G. R. Scott (Eds.), *A companion to dental anthropology* (First ed.) (pp. 142–158). Wiley.

Hillson, S. (1996). *Dental anthropology*. Cambridge University Press. https://doi.org/10.1017/CBO9781139170697

Hillson, S. (2005). *Teeth* (Second ed.). Cambridge University Press. https://doi.org/10.1017/CBO9780511614477

Hodson, C. M., & Gowland, R. (2020). Like mother, like child: Investigating perinatal and maternal health stress in post-medieval London. In R. Gowland & S. Halcrow (Eds.), *The mother-infant nexus in anthropology: Small beginnings, significant outcomes* (Vol. 2019) (pp. 39–64). Springer.

Höss, M., Jaruga, P., Zastawny, T. H., Dizdaroglu, M., & Pääbo, S. (1996). DNA damage and DNA sequence retrieval from ancient tissues. *Nucleic Acids Research*, *24*, 1304–1307. https://doi.org/10.1093/nar/24.7.1304

Hunter, J. P., Guatelli-Steinberg, D., Weston, T. C., Durner, R., & Betsinger, T. K. (2010). Model of tooth morphogenesis predicts Carabelli cusp expression, size, and symmetry in humans. *PLoS ONE*, *5*(7), e11844. https://doi.org/10.1371/journal.pone.0011844

Jernvall, J. (2000). Linking development with generation of novelty in mammalian teeth. *Proceedings of the National Academy of Sciences*, *97*, 2641–2645.

Jernvall, J., & Jung, H.-S. (2000). Genotype, phenotype, and developmental biology of molar tooth characters. *Yearbook of Physical Anthropology*, *43*, 171–190.

Kendall, D. G. (1984). Shape-manifolds, procrustean metrics and complex projective spaces. *Bulletin of the London Mathematical Society*, *16*, 81–121. https://doi.org/10.1112/blms/16.2.81

Kent, J., & Mardia, K. (2001). Shape, Procrustes tangent projections and bilateral symmetry. *Biometrika*, *88*(2), 469–485. https://doi.org/10.1093/biomet/88.2.469

Kenyhercz, M. W., Klales, A. R., & Kenyhercz, W. E. (2014). Molar size and shape in the estimation of biological ancestry: A comparison of relative cusp location using geometric morphometrics and interlandmark distances. *American Journal of Physical Anthropology*, *153*, 269–279.

Klaus, H. D. (2014). Frontiers in the bioarchaeology of stress and disease: Cross-disciplinary perspectives from pathophysiology, human biology, and epidemiology. *American Journal of Physical Anthropology*, *155*, 294–308. https://doi.org/10.1002/ajpa.22574

Klingenberg, C. P. (2015). Analysing fluctuating asymmetry with geometric morphometrics: Concepts, methods, and applications. *Symmetry*, *7*, 843–934. https://doi.org/10.3390/sym7020843

Klingenberg, C. P. (2020). Walking on Kendall's shape space: Understanding shape spaces and their coordinate systems. *Evolutionary Biology*, *47*, 334–352. https://doi.org/10.1007/s11692-020-09513-x

Klingenberg, C. P., & McIntyre, G. S. (1998). Geometric morphometrics of developmental instability: Analyzing patterns of fluctuating asymmetry with Procrustes methods. *Evolution*, *52*(5), 1363–1375. https://doi.org/10.2307/2411306

Lazić, M. M., Carretero, M. A., Crnobrnja-Isailović, J., & Kaliontzopoulou, A. (2015). Effects of environmental disturbance on phenotypic variation: An integrated assessment of canalization, developmental stability, modularity, and allometry in lizard head shape. *American Naturalist*, *185*, 44–58. https://doi.org/10.1086/679011

Leung, B., & Forbes, M. R. (1996). Fluctuating asymmetry in relation to stress and fitness: Effects of trait type as revealed by meta-analysis. *Écoscience*, *3*(4), 400–413. https://doi.org/10.1080/11956860.1996.11682357

Lewis, M. (2017). Fetal paleopathology: an impossible discipline? In S. Han, T. K. Betsinger, & A. B. Scott (Eds.), *The anthropology of the fetus: Biology, culture, and society* (pp. 112–131). Berghan. https://doi.org/10.2307/j.ctvw04h7z.11

Lopuhaa, C. E., Roseboom, T. J., Osmond, C., Barker, D. J. P., Ravelli, A. C. J., Bleker, O. P., van der Zee, J. S., & van der Meulen, J. H. P. (2000). Atopy, lung function and obstructive airways disease in adults after prenatal exposure to the Dutch famine. *Thorax*, *55*, 555–561. https://doi.org/10.1136/thorax.55.7.555

Lynnerup, N., & Klaus, H. D. (2019). Fundamentals and Human Bone and Dental Biology: Structure, Function and Development. In J. E. Buikstra (Ed.), *Ortner's identification of pathological conditions in human skeletal remains* (pp. 35–58). Academic Press. https://doi.org/10.1016/B978-0-12-809738-0.00004-1

Mahoney Swales, D. (2019). A biocultural analysis of mortuary practices in the later Anglo-Saxon to Anglo-Norman Black Gate cemetery, Newcastle-upon-Tyne, England. *International Journal of Osteoarchaeology*, *29*, 198–219. https://doi.org/10.1002/oa.2729

McKillup, S. (2012). *Statistics explained: An introductory guide for life scientists* (Second ed.). Cambridge University Press. https://doi.org/10.1017/CBO9781139047500

Møller, A. P. (1999). Asymmetry as a predictor of growth, fecundity and survival. *Ecology Letters*, *2*, 149–156. https://doi.org/10.1046/j.1461-0248.1999.00059.x

Mullins, S. K., & Taylor, P. J. (2002). The effects of parallax on geometric morphometric data. *Computers in Biology and Medicine*, *32*, 455–464.

Murrar, S., & Brauer, M. (2018). Mixed Model Analysis of Variance. In B. B. Frey (Ed.), *The SAGE encyclopaedia of educational research, measurement, and evaluation* (pp. 1075–1078). Sage.

Noss, J. F., Scott, G. R., Yap Potter, R. H., & Dahlberg, A. A. (1983). Fluctuating asymmetry in molar dimensions and discrete morphological traits in Pima Indians. *American Journal of Physical Anthropology*, *61*, 437–445. https://doi.org/10.1002/ajpa.1330610406

O'Donnell, L., & Moes, E. (2020). Increased dental fluctuating asymmetry is associated with active skeletal lesions, but not mortality hazards in the precontact Southwest United States. *American Journal of Physical Anthropology*, *175*, 156–171. https://doi.org/10.1002/ajpa.24202

Olsen, A.M. (2015). *Digitizing with StereoMorph how to collect 2D landmark and curve data from photographs using the StereoMorph digitizing app*. R Package Version 1.6.1.

Olsen, A. M., & Westneat, M. W. (2015). StereoMorph: An R package for the collection of 3D landmarks and curves using a stereo camera set-up. *Methods in Ecology and Evolution*, *6*, 351–356. https://doi.org/10.1111/2041-210X.12326

Orr, H. A. (2009). Fitness and its role in evolutionary genetics. *Nature Reviews. Genetics*, *10*(8), 531–539. https://doi.org/10.1038/nrg2603

Oxilia, G., Sartorio, J. C. M., Bortolini, E., Zampirolo, G., Papini, A., Boggioni, M., Martini, S., Marciani, F., Arrighi, S., Figus, C., Marciani, G., Romandini, M., Silvestrini, S., Pedrosi, M. E., Mori, T., Riga, A., Kullmer, O., Sarig, R., Fiorenza, L., … Benazzi, S. (2021). Exploring directional and fluctuating asymmetry in the human palate during growth. *American Journal of Physical Anthropology*, *175*(4), 1–18. https://doi.org/10.1002/ajpa.24293

Palmer, A. R. (1994). Fluctuating asymmetry analyses: A primer. In T. A. Markow (Ed.), *Developmental instability: Its origins and evolutionary implications* (pp. 335–364). Kluwer. https://doi.org/10.1007/978-94-011-0830-0_26

Palmer, A. R., & Strobeck, C. (1986). Fluctuating asymmetry: Measurement, analysis, patterns. *Annual Review of Ecology and Systematics*, *17*, 391–421. https://doi.org/10.1146/annurev.es.17.110186.002135

Palmer, A. R., & Strobeck, C. (2003). Fluctuating asymmetry analyses revisited. In M. Polak (Ed.), *Developmental instability (DI): Causes and consequences* (pp. 279–319). Oxford University Press. https://doi.org/10.1093/oso/9780195143454.003.0017

Perez, S. I., Bernal, V., & Gonzalez, P. N. (2006). Differences between sliding semi-landmark methods in geometric morphometrics, with an application to human craniofacial and dental variation. *Journal of Anatomy*, *208*, 769–784. https://doi.org/10.1111/j.1469-7580.2006.00576.x

Perzigian, A. J. (1977). Fluctuating dental asymmetry: Variation among skeletal populations. *American Journal of Physical Anthropology*, *47*, 81–88. https://doi.org/10.1002/ajpa.1330470114

Primeau, C., Arge, S. O., Boyer, C., & Lynnerup, N. (2015). A test of inter- and intra-observer error for an atlas method of combined histological data for the evaluation of enamel hypoplasia. *Journal of Archaeological Science: Reports*, *2*, 384–388.

Pruvost, M., Grange, T., & Geigl, E. M. (2005). Minimizing DNA contamination by using UNG-coupled quantitative real-time PCR on degraded DNA samples: Application to ancient DNA studies. *BioTechniques*, *38*, 569–575. https://doi.org/10.2144/05384ST03

Quade, L., Chazot, P. L., & Gowland, R. (2020). Desperately seeking stress: A pilot study of cortisol in archaeological tooth structures. *American Journal of Physical Anthropology*, *173*(3), 1–10.

R Core Team. (2023). *R: A language and environment for statistical computing*. R Foundation for Statistical Computing. https://www.R-project.org/

Radwan, J., Watson, P. J., Farslow, J., & Thornhill, R. (2003). Procrustean analysis of fluctuating asymmetry in the bulb mite *Rhizoglyphus robini* Claparede (Astigmata: Acaridae). *Biological Journal of the Linnean Society*, *80*, 499–505. https://doi.org/10.1046/j.1095-8312.2003.00249.x

Ravelli, A. C. J., van der Meulen, J. H. P., Michels, R. P. J., Osmond, C., Barker, D. J. P., Hales, C. N., & Bleker, O. P. (1998). Glucose tolerance in adults after prenatal exposure to the Dutch famine. *Lancet*, *35*, 173–177.

Raynor, C., McCarthy, R., & Clough, S. (2011). *Coronation street, South Shields, Tyne And Wear*. Archaeological Excavation and Osteological Analysis Report, Oxford Archaeology North.

Riga, A., Belcastro, M. G., & Moggi-Cecchi, J. (2014). Environmental stress increases variability in the expression of dental cusps. *American Journal of Physical Anthropology*, *153*, 397–407. https://doi.org/10.1002/ajpa.22438

Robinson, D. L., Blackwell, P. G., Stillman, E. C., & Brook, A. H. (2002). Impact of landmark reliability on the planar Procrustes analysis of tooth shape. *Archives of Oral Biology*, *47*, 545–554. https://doi.org/10.1016/S0003-9969(02)00038-9

Rohlf, F. J. (1999). Shape statistics: Procrustes superimpositions and tangent spaces. *Journal of Classification*, *16*, 197–223. https://doi.org/10.1007/s003579900054

Roseboom, T. J., van der Meulen, J. H. P., Osmond, C., Barker, D. J. P., Ravelli, A. C. J., Schroeder-Tanka, J. M., van Montfrans, G. A., Michels, R. P. J., & Bleker, O. P. (2000). Coronary heart disease in adults after prenatal exposure to the Dutch famine. *Heart*, *84*, 595–598. https://doi.org/10.1136/heart.84.6.595

Roseboom, T. J., van der Meulen, J. H. P., & Ravelli, A. C. J. (2001). Effects of prenatal exposure to the Dutch famine on adult disease in later life: An overview. *Molecular and Cellular Endocrinology*, *185*, 93–98. https://doi.org/10.1016/S0303-7207(01)00721-3

Salazar-Ciudad, I., & Jernvall, J. (2002). A gene network model accounting for development and evolution of mammalian teeth. *Proceedings of the National Academy of Sciences*, *99*, 8116–8120. https://doi.org/10.1073/pnas.132069499

Savriama, Y., & Klingenberg, C. P. (2011). Beyond bilateral symmetry: Geometric morphometric methods for any type of symmetry. *BMC Evolutionary Biology*, *11*, 280. https://doi.org/10.1186/1471-2148-11-280

Schaefer, M., Black, S., & Scheuer, L. (2009). *Juvenile osteology: A laboratory and Field manual*. Elsevier.

Scheuer, L., & Black, S. (2000). *Developmental juvenile osteology*. Academic Press. https://doi.org/10.1016/B978-012624000-9/50004-6

Schmalhausen, I. I. (1949). *Factors of evolution*. Blakiston.

Selye, H. (1973). The evolution of the stress concept. *American Scientist*, *61*, 692–699.

Shearer, B. M., Cooke, S. B., Halenar, L. B., Reber, S. L., Plummer, J. E., Delson, E., & Tallman, M. (2017). Evaluating causes of error in landmark-based data collection using scanners. *PLoS ONE*, *12*(11), e0187452. https://doi.org/10.1371/journal.pone.0187452

Silva, M. F. S., De Andrade, I. M., & Mayo, S. J. (2012). Geometric morphometrics of leaf blade shape in *Montrichardia linifera (Araceae)* populations from the Rio Parnaíba Delta, north-East Brazil. *Botanical Journal of the Linnean Society*, *170*(4), 554–572. https://doi.org/10.1111/j.1095-8339.2012.01309.x

Smith, D. R., Crespi, B., & Bookstein, F. L. (1997). The Procrustes method and fluctuating asymmetry in the honey bee, *Apis mellifera*: Effects of ploidy and hybridization. *Journal of Evolutionary Biology*, *10*, 551–574.

Stinson, S. (1985). Sex differences in environmental sensitivity during growth and development. *Yearbook of Physical Anthropology*, *28*, 123–147. https://doi.org/10.1002/ajpa.1330280507

Temple, D. H. (2014). Plasticity and constraint in response to early-life stressors among late/final Jomon period foragers from Japan: Evidence for life history trade-offs from incremental microstructures of enamel. *American Journal of Physical Anthropology*, *155*, 537–545. https://doi.org/10.1002/ajpa.22606

Townsend, G. C. (1981). Fluctuating asymmetry in the deciduous dentition of Australian Aboriginals. *Journal of Dental Research*, *60*(11), 1849–1857. https://doi.org/10.1177/00220345810600110401

Townsend, G. C., & Brown, T. (1980). Dental asymmetry in Australian Aboriginals. *Human Biology*, *52*(4), 661–673.

Townsend, G. C., Richards, L., & Hughes, T. (2003). Molar intercuspal dimensions: Genetic input to phenotypic variation. *Journal of Dental Research*, *82*, 350–355. https://doi.org/10.1177/154405910308200505

Uzunov, T. T., Kosturkov, D., Uzunov, T., Filchev, D., Bonev, B., & Filchev, A. (2015). Registration of internal morphological characteristics of the tooth using dental photography. *Journal of International Medical Association Bulgaria*, *22*(1), 677–681. https://doi.org/10.5272/jimab.2015211.677

Vaiserman, A. M. (2015). Epigenetic programming by early-life stress: Evidence from human populations. *Developmental Dynamics*, *244*, 254–265. https://doi.org/10.1002/dvdy.24211

Van Pool, T. L., & Leonard, R. D. (2010). *Quantitative analysis in archaeology*. Wiley-Blackwell.

Van Valen, L. (1962). A study of fluctuating asymmetry. *Evolution*, *16*, 125–142. https://doi.org/10.1111/j.1558-5646.1962.tb03206.x

Vaupel, J. W. (1988). Inherited frailty and longevity. *Demography*, *25*(2), 277–287. https://doi.org/10.2307/2061294

Waddington, C. H. (1957). *The strategy of the genes*. George Allen Unwin.

Wasiljew, B. D., Pfaender, J., Wipfler, B., Utama, I. V., & Herder, F. (2020). Do we need the third dimension? Quantifying the effect of the z-axis in 3D geometric morphometrics based on sailfin silversides (Telmatherinidae). *Journal of Fish Biology*, *97*(2), 537–545. https://doi.org/10.1111/jfb.14410

Watanabe, A. (2018). How many landmarks are enough to characterize shape and size variation? *PLoS ONE*, *13*(6), e0198341. https://doi.org/10.1371/journal.pone.0198341

Webb, E., Thomson, S., Nelson, A., White, C., Koren, G., Rieder, M., & Van Uum, S. (2010). Assessing individual systemic stress through cortisol analysis of archaeological hair. *Journal of Archaeological Science*, *37*(4), 807–812. https://doi.org/10.1016/j.jas.2009.11.010

Weston, D. (2008). Investigating the specificity of periosteal reactions in pathology museum specimens. *American Journal of Physical Anthropology*, *137*(1), 48–59. https://doi.org/10.1002/ajpa.20839

White, T. D., & Folkens, P. A. (2005). *The human bone manual*. Elsevier.
Wood, B. A., Abbott, S. A., & Graham, S. H. (1983). Analysis of the dental morphology of Plio-Pleistocene hominids II. Mandibular molars—Study of cusp areas, fissure pattern and cross-sectional shape of the crown. *Journal of Human Anatomy*, *137*(2), 287–314.
Wood, B. A., & Engleman, C. A. (1988). Analysis of the dental morphology of Plio-Pleistocene hominids. V. Maxillary postcanine tooth morphology. *Journal of Human Anatomy*, *161*, 1–35.
Wood, J. W., Milner, G. R., Harpending, H. C., & Weiss, K. M. (1992). The osteological paradox: Problems of inferring prehistoric health from skeletal samples. *Current Anthropology*, *33*, 343–370. https://doi.org/10.1086/204084
Zelditch, M. L., & Swiderski, D. L. (2018). *A practical companion to geometric Morphometrics for biologists: Running analyses in freely-available software* (Second ed.). Academic Press.
Zelditch, M. L., Swiderski, D. L., & Sheets, H. D. (2012). *Geometric morphometrics for biologists. A primer*. Academic Press.

SUPPORTING INFORMATION

Additional supporting information can be found online in the Supporting Information section at the end of this article.

How to cite this article: Wigley, B., Stillman, E., & Craig-Atkins, E. (2024). Taking shape: A new geometric morphometric approach to quantifying dental fluctuating asymmetry and its application to the evaluation of developmental stress. *Archaeometry*, 1–25. https://doi.org/10.1111/arcm.12973